BULK OBSERVABLES, LONG-RANGE CORRELATIONS AND FLOW IN pp COLLISIONS AT LHC*

L. Bravina[a], R. Kolevatov[a], L. Malinina[a,b]
M.S. Nilsson[a], E. Zabrodin[a,b]

[a]Department of Physics, University of Oslo, PB 1048, 0316 Oslo, Norway
[b]Skobeltzyn Institute for Nuclear Physics, Moscow State University
119899 Moscow, Russia

(Received December 27, 2011)

Bulk observables like multiplicity, rapidity and transverse momentum distributions of hadrons produced both in inelastic and non-diffractive pp collisions at energies from $\sqrt{s} = 200$ GeV to 7 TeV are described within the Monte Carlo quark-gluon string model. The short-range correlations of particles in the strings and interplay between the multi-string processes at ultra-relativistic energies lead to violation of Feynman scaling at midrapidity. Model predicts strong increase of the slope with energy in forward–backward multiplicity dependence $\langle n_{\rm F}(n_{\rm B})\rangle$ due to long-range correlations between particles produced in the multi-string processes. The comparison of model results on pion–pion femtoscopic correlations with the experimental data favors significant decrease of particle formation time with rising collision energy. The possibility to produce anisotropic flow on the initial stages of pp reactions, both directed v_1 and elliptic v_2, from the decay of the strings is discussed.

DOI:10.5506/APhysPolBSupp.5.419
PACS numbers: 25.75.Gz, 24.10.Lx, 13.85.–t, 12.40.Nn

1. Introduction

One of the goals of CERN experiments at LHC is a search for signals of the hot and dense matter created in relativistic heavy ion collisions. The main signatures of such matter are considered to be *e.g.* jet quenching, strong anisotropic flow and ridge. These effects were found in Au + Au collisions at $\sqrt{s} = 200$ AGeV at RHIC. Similar effects, detected at LHC at energies of one order of magnitude higher, $\sqrt{s} = 2.76$ ATeV, showed that the density of the matter becomes larger, the particle multiplicities and magnitude of anisotropic flow are growing gradually but not very significantly. High

* Presented at the Conference "Strangeness in Quark Matter 2011", Kraków, Poland, September 18–24, 2011.

multiplicity pp data at $\sqrt{s} = 7$ TeV reveal the presence of near-side ridge similar to that detected in Au–Au collisions at RHIC. They also show the possible existence of radial flow in identified particle p_{T} spectra, dependent on m_{T} of the particle, which was supported by femtoscopic radii of the particles. The scientists put forward the idea that hot and dense matter with very particular properties can be created also in central pp collisions at very high energies. For theoretical models it means that these collective effects in pp collisions can be described by hydrodynamics, usually applied only to nucleus–nucleus collisions, where the matter with many degrees of freedom is formed. The question arises whether it can also be explained by initial state effects as was suggested within the Gribov's Reggeon Field Theory (GRT) [1]. In the present paper, we discuss the predictions of Quark Gluon String Model (QGSM) [2] for pp collisions at RHIC and LHC energies. The QGSM is based on the GRT accomplished by the string phenomenology. Its brief description is given in the next section.

2. Basic features of the model

The QGSM is based on the $1/N$ expansion, where N is number of colors or flavors, of the amplitude for a QCD process. The diagrams arising in this approach correspond to processes with the exchange of Regge singularities in the t-channel and, therefore, can be calculated within the perturbative GRT. The theoretically obtained statistical weights, structure functions of hadrons and fragmentation functions of leading quarks are utilized in the present Monte Carlo version of the QGSM [3] to choose the subprocesses of hadronic interactions, to calculate the mass and momentum of each string and, finally, to simulate the string fragmentation into hadrons.

As independent degrees of freedom the QGSM includes the nonets of vector and pseudoscalar mesons, the baryon octet and decuplet, and their antistates. Pauli blocking of occupied final states is implemented by excluding the already occupied final states from the available phase space. Strings in the QGSM can be produced as a result of both the momentum transfer (diffraction) and color exchange mechanism. The Pomeron, which is a pole with an intercept $\alpha_{\mathbb{P}}(0) > 1$ in the GRT, corresponds to the cylinder-type diagrams. The s-channel discontinuities of the diagrams, representing the exchange by n-Pomerons, are related to process of $2k$ $(k \leq n)$ string production. If the contributions of all n-Pomeron exchanges to the forward elastic scattering amplitude are known, the AGK cutting rules [4] enable one to determine the cross sections for $2k$-strings. The hard gluon–gluon scattering and semi-hard processes with quark and gluon interactions are also incorporated in the model via the so-called hard Pomeron exchange. Its presence seems to be necessary to describe the rise of multiplicity at midrapidity and p_{T} spectra of secondaries in pp interactions at LHC within the QGSM [5].

For the modeling of string fragmentation the Field–Feynman algorithm [7] is employed. It enables one to consider emission of hadrons from both ends of the string with equal probabilities. The break-up procedure invokes the energy-momentum conservation and the preservation of the quark numbers. Due to the uncertainty principle it takes some time to create a hadron from constituent quarks, *e.g.*, fast particles are created the last. In string models two definitions of formation time are accepted [8]: the time when the string is broken and all constituents of the hadron are created (constituent) or the time when the trajectories of hadron constituents (quarks) cross ("yo–yo"). In this version of QGSM we are using the constituent formation time. Further details of the MC version of QGSM and its extension to $A + A$ collisions can be found in [3, 5, 6].

3. Pseudorapidity and transverse momentum distributions

For the comparison with model calculations the experimental data reported for pp and $\bar{p}p$ collisions in [9, 10, 11, 12, 13] are used. Pseudorapidity distributions of charged particles obtained for inelastic and non-single diffraction (NSD) pp interactions at energies from $\sqrt{s} = 200\,\text{GeV}$ to $14\,\text{TeV}$ are presented in Fig. 1 (a) together with the available experimental data. According to the hypothesis of Feynman scaling the density of charged particles $dN^{\text{ch}}/d\eta$ at midrapidity should be saturated at very high energies. This scaling regime is obviously not reached yet. Moreover, at LHC energies $dN^{\text{ch}}/d\eta\,|_{\eta=0}$ demonstrates a non-linear rise with $\ln s$, as suggested by the saturation of the Froissart bound. For pp collisions at top LHC energy $\sqrt{s} = 14$ TeV the QGSM predicts $dN_{\text{inel}}/d\eta\,|_{\eta=0} = 6.1$, $dN_{\text{NSD}}/d\eta\,|_{\eta=0} = 7.0$, respectively.

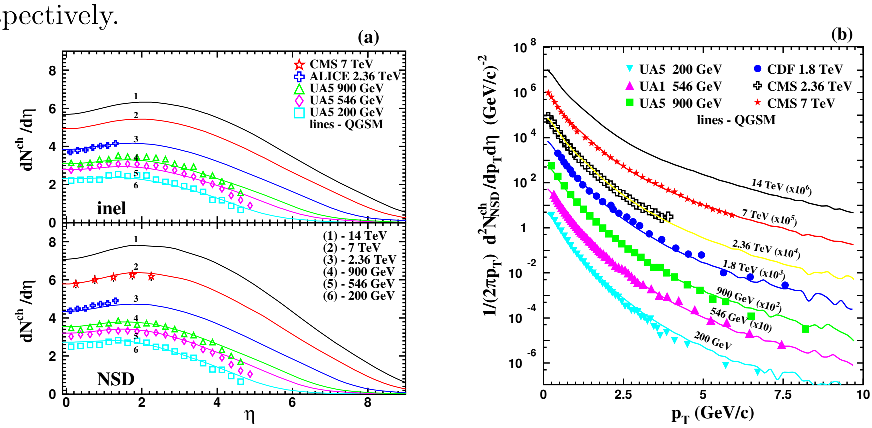

Fig. 1. (Color online) (a) Pseudorapidity spectra for charged particles in inelastic and NSD pp collisions at 200 GeV $\leq \sqrt{s} \leq$ 14 TeV. (b) Transverse momentum distribution of the invariant cross section in NSD pp collisions in the same energy range.

Figure 1 (b) shows the transverse momentum distribution of the invariant cross sections of charged particles in NSD pp events. The contribution of hard processes increases with rising $\sqrt{s}$, therefore, the $p_{\rm T}$ spectra of secondaries become harder, especially at $p_{\rm T} \geq 2.5$ GeV/c. The average transverse momentum of the produced hadrons also increases. For the NSD pp collisions at $\sqrt{s} = 14$ TeV the model predicts $\langle p_{\rm T} \rangle = 0.56 \pm 0.03$ GeV/c.

4. Long-range and femtoscopy correlations

The term "long-range correlations" is used for correlations between charged particles emitted in forward (F) and backward (B) hemispheres. These correlations were first observed experimentally in [9]. The dependencies $\langle n_{\rm B}(n_{\rm F}) \rangle$ of the mean charged-particle multiplicities measured in the pseudorapidity intervals $-4 \leq \eta \leq 0$ and $0 \leq \eta \leq 4$ are shown in Fig. 2 for pp collisions at four different energies. We see good agreement between the model results and the available experimental data. Also, these dependencies are quite linear

$$\langle n_{\rm B}(n_{\rm F}) \rangle = a + b\, n_{\rm F}\,, \tag{1}$$

whereas the slope parameter b increases with the rising energy. Note that hard processes do not alter the observed correlations, *i.e.* the strength of the correlations is fully determined by the processes with increasing number of soft Pomerons.

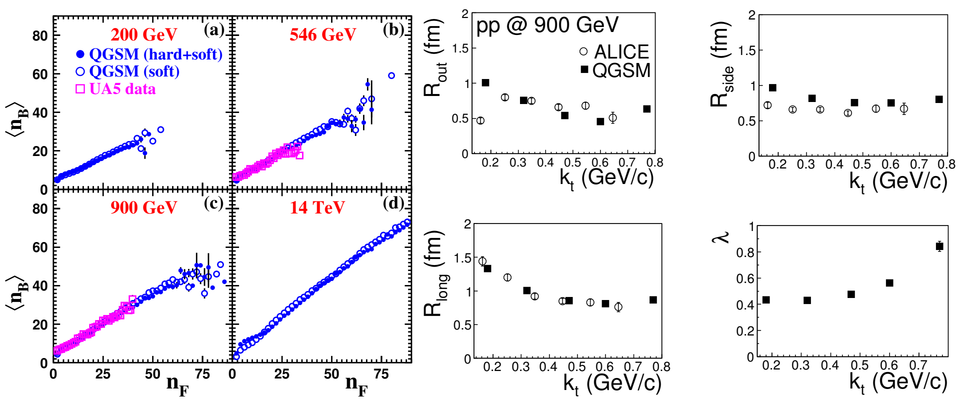

Fig. 2. (Color online) Left: Backward–forward multiplicity correlations $\langle n_{\rm B}(n_{\rm F}) \rangle$ for $0 \leq |\eta| \leq 4$ in NSD pp interactions at $\sqrt{s} = 200$ GeV, 546 GeV, 900 GeV and 14 TeV. Open circles denote contributions of soft processes, full symbols are for all processes, open squares represent UA5 data. Right: Three-dimensional $\pi^+\pi^+$ correlation radii as functions of $k_{\rm T}$ in pp collisions at $\sqrt{s} = 900$ GeV for minimum bias events. Open circles denote ALICE experimental data, full squares present QGSM calculations.

The 3D femtoscopy correlation analysis can provide information about both the form of the emitting source and the duration of the emission [14,15]. Here, the momentum correlation functions are analyzed in terms of the *out*, *side* and *longitudinal* components of the relative momentum vector $\boldsymbol{q} = \{q_{\rm out}, q_{\rm side}, q_{\rm long}\}$, where $q_{\rm out}$ and $q_{\rm side}$ denote the transverse components of the vector $\boldsymbol{q}$, and the direction of $q_{\rm out}$ is parallel to the transverse component of the pair three-momentum. The corresponding correlation widths are usually parametrized in terms of the Gaussian correlation radii

$$\mathrm{CF}(p_1, p_2) = 1 + \lambda \exp\left(-R_{\rm out}^2 q_{\rm out}^2 - R_{\rm side}^2 q_{\rm side}^2 - R_{\rm long}^2 q_{\rm long}^2\right) . \tag{2}$$

The extracted R_i as functions of average pair transverse momentum $k_{\rm T} = |\vec{p_{{\rm t},1}} + \vec{p_{{\rm t},2}}|/2$ are presented in Fig. 2 (b) for the low multiplicity bin in *pp* interactions at $\sqrt{s} = 900$ GeV. One can see that the QGSM points are rather close to the ALICE experimental ones [16]. However, this implies significant reduction of the formation time with increasing energy [17] or, equivalently, rise of the string tension.

5. Directed and elliptic flow in *pp* collisions

The possible formation of anisotropic flow or rather its two first components, directed v_1 and elliptic v_2 flow, in *pp* collisions at LHC energies is a very popular topic nowadays. Several scenarios have been discussed

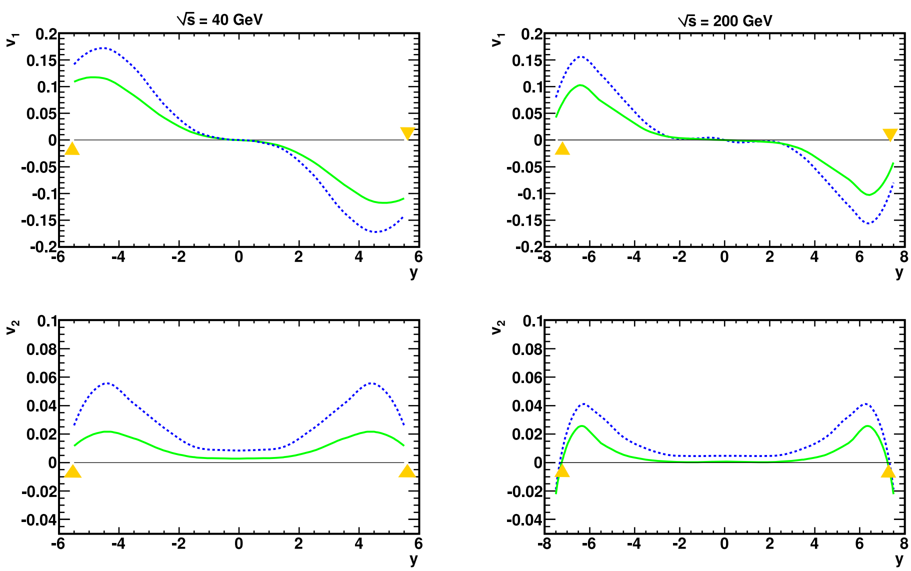

Fig. 3. (Color online) Flow coefficients v_1 and v_2 obtained for a decay of a string with energy $\sqrt{s} = 40$ GeV and 200 GeV and with impact parameters $b = 0.5$ fm (solid lines) and $b = 1.0$ fm (dashed lines).

(see *e.g.* [18] and references therein). In the color exchange mechanism of string excitation, strings are stretching between constituents belonging to different hadrons. Therefore, these strings usually have some slopes in the transverse direction. In [19] the fragmentation of a classical relativistic string with a certain transverse separation of the ends has been considered. It was shown that the fragmentation process of such a string could generate both directed and elliptic flow as displayed in Fig. 3.

This work was supported by the Norwegian Research Council (NFR) under Contract No. 185664/V30.

REFERENCES

[1] V. Gribov, *Sov. Phys. JETP* **26**, 414 (1968); L.V. Gribov, E.M. Levin, M.G. Ryskin, *Phys. Rep.* **100**, 1 (1983).

[2] A.B. Kaidalov, *Phys. Lett.* **B116**, 459 (1982); A.B. Kaidalov, K.A. Ter-Martirosyan, *Phys. Lett.* **B117**, 247 (1982).

[3] N.S. Amelin, L.V. Bravina, *Sov. J. Nucl. Phys.* **51**, 133 (1990).

[4] V. Abramovskii, V. Gribov, O. Kancheli, *Sov. J. Nucl. Phys.* **18**, 308 (1974).

[5] J. Bleibel *et al.*, `arXiv:1011.2703 [hep-ph]`.

[6] L.V. Bravina *et al.*, *Phys. Rev.* **C60**, 044905 (1999); E.E. Zabrodin *et al.*, *Phys. Lett.* **B508**, 184 (2001).

[7] R.D. Field, R.P. Feynman, *Nucl. Phys.* **B136**, 1 (1978).

[8] A. Bialas, M. Gyulassy, *Nucl. Phys.* **B291**, 793 (1987).

[9] G.J. Alner *et al.* [UA5 Collab.], *Phys. Rep.* **154**, 247 (1987).

[10] G. Arnison *et al.* [UA1 Collab.], *Phys. Lett.* **B118**, 167 (1982); C. Albajar *et al.* [UA1 Collab.], *Nucl. Phys.* **B335**, 261 (1990).

[11] F. Abe *et al.* [CDF Collab.], *Phys. Rev. Lett.* **61**, 1819 (1988); *Phys. Rev.* **D41**, 2330 (1990).

[12] K. Aamodt *et al.* [ALICE Collab.], *Eur. Phys. J.* **C68**, 89 (2010); **C68**, 345 (2010); *Phys. Lett.* **B693**, 53 (2010).

[13] K. Khachatryan *et al.* [CMS Collab.], *J. High Energy Phys.* **1002**, 041 (2010); *Phys. Rev. Lett.* **105**, 022002 (2010).

[14] M.I. Podgoretsky, *Fiz. Elem. Chast. Atom. Yadra* **20**, 628 (1989) (in Russian).

[15] R. Lednicky, *Phys. Atom. Nucl.* **67**, 72 (2004).

[16] K. Aamodt *et al.* [ALICE Collab.], *Phys. Rev.* **D82**, 052001 (2010).

[17] M.S. Nilsson *et al.*, *Phys. Rev.* **D84**, 054006 (2011).

[18] D. d'Enterria *et al.*, *Eur. Phys. J.* **C66**, 173 (2010).

[19] R. Kolevatov, *Eur. Phys. J.* **C68**, 513 (2010).